



1 **Assessing Responses and Impacts of Solar climate intervention**  
2 **on the Earth system with stratospheric aerosol injection**  
3 **(ARISE-SAI)**

4

5 Jadwiga H. Richter<sup>1</sup>, Daniele Visioni<sup>2</sup>, Douglas G. MacMartin<sup>2</sup>, David A. Bailey<sup>1</sup>, Nan  
6 Rosenbloom<sup>1</sup>, Walker R. Lee<sup>2</sup>, Mari Tye<sup>1</sup>, Jean-Francois Lamarque<sup>1</sup>

7

8 <sup>1</sup> Climate and Global Dynamics Laboratory, National Center for Atmospheric Research, Boulder CO

9 <sup>2</sup> Sibley School for Mechanical and Aerospace Engineering, Cornell University, Ithaca NY

10

11 *Correspondence to:* Jadwiga H. Richter (jrichter@ucar.edu)

12

13 **Abstract.** Solar climate intervention using stratospheric aerosol injection is a proposed method of reducing global  
14 mean temperatures to reduce some of the consequences of climate change. A detailed assessment of responses and  
15 impacts of such an intervention is needed with multiple global models to support societal decisions regarding the use  
16 of these approaches to help address climate change. We present here a new modeling protocol and a 10-member  
17 ensemble of simulations using one of the most comprehensive Earth system models, aimed at simulating a plausible  
18 deployment of stratospheric aerosol injection and reproducibility of simulations using other Earth system models to  
19 enable community assessment of responses of the Earth system to solar climate intervention. The Assessing  
20 Responses and Impacts of Solar climate intervention on the Earth system with stratospheric aerosol injection  
21 (ARISE-SAI) simulations utilize a moderate emission scenario, introduce stratospheric aerosol injection at ~ 21 km  
22 in year 2035, and keep global mean surface air temperature near 1.5°C above the pre-industrial value (ARISE-SAI-  
23 1.5). We present here the detailed set-up, aerosol injection strategy, and mean surface climate changes in these  
24 simulations so they can be reproduced in other global models.

25 **1 Introduction**

26 Solar climate intervention (SCI), or solar geoengineering, is a proposed strategy that could potentially reduce the  
27 adverse effects on weather and climate associated with climate change by increasing the reflection of sunlight by  
28 particles and clouds in the atmosphere. The recent National Academies of Sciences, Engineering and Medicine  
29 (NASEM) report on solar geoengineering research and governance (NASEM, 2021) calls for increased research to  
30 understand the benefits, risks and impacts of various SCI approaches. Stratospheric aerosol injection (SAI) has been  
31 shown to be a promising method of global climate intervention in terms of restoring climate to present day conditions  
32 (e.g.: Tilmes et al., 2018; MacMartin et al. 2019; Simpson et al., 2019). However, there still exist large uncertainties



33 in climate response and impacts (NASEM, 2021, Kravitz and MacMartin, 2020), and ensuing human and ecological  
34 impacts (Carlson and Trisos, 2018). Due to the large internal variability of Earth's climate, the evaluation of SCI risks  
35 and impacts requires large ensembles of simulations (Deser et al., 2012; Kay et al., 2015; Maher et al., 2021) and  
36 Earth system models (ESMs) capable of simulating the key processes and interactions between multiple Earth system  
37 components, including prognostic aerosols, interactive chemistry, and coupling between the atmosphere, land, ocean,  
38 and sea ice. For studies of climate intervention using SAI, an accurate representation of the entire stratosphere,  
39 including dynamics and chemistry, is needed to capture the transport of aerosols and their interactions with  
40 stratospheric constituents such as water vapor and ozone (e.g.: Pitari et al., 2014).

41 The Geoengineering Model Intercomparison Project (GeoMIP) for many years has facilitated inter-model  
42 comparisons of possible climate responses to SCI to examine where model responses to geoengineering were robust  
43 and identify areas of large uncertainty. However, in order to ensure participation from multiple ESMs, the design of  
44 GeoMIP simulations has often been simplified by utilizing solar constant reduction (Kravitz et al., 2013; Kravitz et  
45 al., 2021) or prescription of an aerosol distribution (Tilmes et al., 2015) or a spatially uniform injection rate of SO<sub>2</sub>  
46 (i.e. continuous injection from 10°N to 10°S in the most recent G6sulfur experiments (Vioni et al., 2021b). Vioni  
47 et al. (2021a) showed that solar dimming does not produce the same surface climate effects as simulating aerosols in  
48 the stratosphere. Kravitz et al. (2019) showed that strategically injecting SO<sub>2</sub> at multiple locations to maintain more  
49 than one climate target may reduce some of the projected side-effects by more evenly cooling at all latitudes; hence,  
50 model experiments with plausible implementation of SCI are needed in order to assess risks and benefits of these  
51 strategies. The Geoengineering Large Ensemble (GLENS, Tilmes et al. 2018), which used version 1 of the  
52 Community Earth System Model with the Whole Atmosphere Community Climate Model as its atmospheric  
53 component (CESM1(WACCM), Mills et al. 2017), was the first large-ensemble (20-member) set of climate  
54 intervention simulations carried out with a single ESM that interactively represented many of the key processes  
55 relevant to SAI and has provided a community dataset for the examination of potential impact of SAI on mean  
56 climate and variability. GLENS utilized sulfur dioxide (SO<sub>2</sub>) injections that were strategically placed every year to  
57 keep the global mean temperature, equator-to-pole, and pole-to-pole temperature gradients near 2020 levels in an  
58 effort to minimize the surface temperature impacts of this intervention. However, GLENS has several experimental  
59 design issues that are not aligned with realistic projections for Earth system outcomes that would provide more  
60 accurate representation of possible real-world effects and impacts. Firstly, GLENS adopted a high emission scenario  
61 of RCP8.5 until 2100, requiring a very large amount of stratospheric aerosols by the end of the century to offset the  
62 continuously increasing emissions. Estimates for future emissions based on current commitments are lower than  
63 RCP8.5 (Hausfather and Peters, 2020), and thus impact analyses, especially based on the last two decades of the  
64 GLENS, are likely to overestimate the risks and adverse impacts of SAI. Additionally, in the GLENS simulations,  
65 intervention commenced in 2020, adding another unrealistic element from a real-world standpoint. Furthermore,  
66 SO<sub>2</sub> injections were at 23-25 km altitude, which is technologically more difficult to achieve than a lower altitude  
67 injection (Bingaman et al. 2020).

68 Tilmes et al. (2020) has carried out simulations with SO<sub>2</sub> injections with CESM2(WACCM6) and GLENS-  
69 like set-up for the Shared Socioeconomic Pathway SSP5-8.5 and SSP5-3.4-OS scenarios (O'Neill et al., 2016). Here



70 we describe a new set-up of an ensemble of simulations with CESM2(WACCM6) designed to simulate a more  
71 plausible implementation scenario of SCI using SAI that can be replicated by other modeling centers, and present  
72 preliminary diagnostics to begin enabling community assessment of responses of the Earth system to such an  
73 intervention.

## 74 **2 Methods**

75

### 76 **2.1 Model Description**

77 For all simulations presented here, we utilize here the newest, most comprehensive version of the NCAR  
78 whole atmosphere ESM, the Community Earth System Model, version 2 with the Whole Atmosphere Community  
79 Climate Model version 6 as its atmospheric component (CESM2(WACCM6), Gettelman et al., 2019; Danabasoglu  
80 et al., 2020). CESM2(WACCM6) was used to contribute climate change projection simulations to the Coupled  
81 Model Intercomparison Project Phase 6 (CMIP6) (Eyring et al., 2016). CESM2(WACCM6) has numerous  
82 improvements to all its components, including fully interactive tropospheric chemistry and an interactive crop model  
83 as compared to CESM1(WACCM) (Mills et al., 2017).

84 CESM2(WACCM6) is a fully coupled ESM with prognostic atmosphere, land, ocean, sea-ice, land-ice,  
85 river and wave components. The atmospheric model, WACCM6, uses a finite volume dynamical core with  
86 horizontal resolution of  $1.25^\circ$  longitude by  $0.9^\circ$  latitude. WACCM6 includes 70 vertical levels with a model top at  
87  $4.5 \times 10^6$  hPa ( $\sim 140$  km). Tropospheric physics in WACCM6 are the same as in the lower top configuration, the  
88 Community Atmosphere Model version 6 (CAM6) and use the Zhang and McFarlane (1995) convection  
89 parameterization, the Cloud Layers Unified By Binormals (CLUBB; Golaz et al., 2002; Larson, 2017) unified  
90 turbulence scheme, and the updated Morrison-Gettelman microphysics scheme (MG2; Gettelman & Morrison,  
91 2015). A form drag parameterization of Beljaars et al. (2004) and an anisotropic gravity wave drag scheme  
92 following Scinocca and McFarlane (2000) are now used in place of the turbulent mountain stress parameterization  
93 that was used in CESM1. CESM2(WACCM6) includes a parameterization of non-orographic waves which follows  
94 Richter et al. (2010) with changes to tunable parameters described in Gettelman et al. (2019). Parameterized gravity  
95 waves are a substantial driver of the quasi-biennial oscillation (QBO) which is internally-generated in  
96 CESM2(WACCM6). CESM2(WACCM6) includes prognostic aerosols which are represented using the Modal  
97 Aerosol Model version 4 (MAM4) as described in Liu et al. (2016). CESM2(WACCM6) also includes a  
98 comprehensive chemistry module with interactive tropospheric, stratospheric, mesospheric and lower thermospheric  
99 chemistry (TSMLT) with 228 prognostic chemical species, described in detail in Gettelman et al. (2019).

100 The ocean model in CESM2(WACCM6) is based on the Parallel Ocean Program version 2 (POP2; Smith et  
101 al., 2010; Danabasoglu et al., 2012), but contains many advances since its version in CESM1. These include a new  
102 parameterization for mixing effects in estuaries, increased mesoscale eddy (isopycnal) diffusivities at depth, use of  
103 prognostic chlorophyll for shortwave absorption, use of salinity-dependent freezing point together with the sea ice  
104 model, and a new Langmuir mixing parameterization in conjunction with the new wave model component  
105 (Danabasoglu et al., 2020). The horizontal resolution of POP2 is uniform in the zonal direction ( $1.125^\circ$ ), and varies



106 from  $0.64^\circ$  (occurring in the Northern Hemisphere) to  $0.27^\circ$  at the Equator. In the vertical, there are 60 levels with a  
107 uniform resolution of 10 m in the upper 160m. The ocean biogeochemistry is represented using the Marine  
108 Biogeochemistry Library (MARBL), which is an updated implementation of the Biochemistry Elemental Cycle  
109 (Moore et al., 2002; 2004; 2013). CESM2 uses version 3.14 of the NOAA WaveWatch-III ocean surface wave  
110 prediction model (Tolman, 2009). Sea-ice in CESM2(WACCM6) is represented using CICE version 5.1.2 (CICE5;  
111 Hunke et al., 2015) and uses the same horizontal grid as POP2. The vertical resolution of sea-ice has been enhanced  
112 to eight layers, from four in CESM1. The snow model resolves three layers, and the melt pond parameterization has  
113 been updated (Hunke et al., 2013).

114 CESM2(WACCM6) uses the Community Land Model version 5 (CLM5) (Lawrence et al., 2019). As  
115 compared to CLM4, CLM5 includes improvements to soil hydrology, spatially explicit soil depth, dry surface layer  
116 control on soil evaporation, and an updated ground-water scheme, as well as several snow model updates. CLM5  
117 includes a global crop model that treats planting, harvest, grain fill, and grain yields for six crop types (Levis et al.,  
118 2018), a new fire model (Li et al., 2013; Li and Lawrence, 2017), multiple urban classes and an updated urban  
119 energy model (Oleson & Feddema, 2019), and improved representation of plant dynamics. The river transport model  
120 used is the Model for Scale Adaptive River Transport (MOSART; H. Y. Li et al., 2013).

121

## 122 **2.2 Reference simulations**

123 We use the moderate Shared Socioeconomic Pathway scenario of SSP2-4.5 for our simulations, which more closely  
124 captures current policy scenarios compared to higher emission scenarios such as SSP5-8.5 (Burgess et al., 2020).  
125 SSP2-4.5, which marks a continuation of the Representative Concentration Pathway 4.5 (RCP4.5) scenario, is a  
126 “middle-of-the-road,” intermediate mitigation scenario where “the world follows a path in which social, economic,  
127 and technological trends to not shift markedly from historical patterns” (O’Neill et al., 2017), representing the  
128 medium range of future forcing pathways (O’Neill et al., 2016). A 5-member reference ensemble with  
129 CESM2(WACCM6) and the SSP2-4.5 scenario was carried out as part of the CMIP6 project for years 2015 - 2100.  
130 Surface temperature evolution and equilibrium climate sensitivity in these simulations are described in detail in  
131 Meehl et al. (2020). We carried out an additional 5-member ensemble of these simulations from years 2015 - 2069  
132 with augmented high-frequency output for high-impact event analysis, as well as additional output for the land  
133 model to match the SCI simulations. The additional 5-member ensemble was branched from the three existing  
134 historical CESM2(WACCM6) simulations in the same manner as the first 5-member ensemble, but with an addition  
135 of small temperature perturbations for each ensemble member ( $[6, 7, 8, 9, 10] \times 10^{-14}$  K, respectively), at the first  
136 model timestep. CESM2 ranks highly against other CMIP6 models in the ability to represent large scale circulations  
137 and key features of tropospheric climate over the historical time period (e.g.: Simpson et al., 2020; Duviver et al.,  
138 2020; Coburn and Pryor 2021).

139

## 140 **2.3 Climate intervention simulations**

141 We carried out a 10-member ensemble of SAI simulations with CESM2(WACCM) designed to simulate a plausible  
142 implementation scenario of SCI using SAI for evaluation of potential climate intervention risks and impacts. These



143 simulations are the first of a planned set of different SCI implementation scenarios; we denote the entire planned set  
144 of simulations as “Assessing Responses and Impacts of Solar climate intervention on the Earth system,” or  
145 “ARISE,” with simulations of SAI denoted “ARISE-SAI”. The first ARISE-SAI simulations, presented here, utilize  
146 a moderate emission scenario, SSP2-4.5 (O’Neill et al., 2016), and begin intervention in 2035 by applying SAI to  
147 cool the Earth with the target of maintaining global surface temperatures of  $\sim 1.5^{\circ}\text{C}$  above preindustrial levels, the  
148 target proposed in the 2015 Paris agreement and described by the IPCC as a possibly important threshold for climate  
149 safety (IPCC 2018). The simulation set is called ARISE-SAI-1.5. Subsequent ARISE-SAI simulations are planned  
150 with varying temperature targets and start dates. Sulfur dioxide injections in the ARISE-SAI-1.5 simulations are  
151 placed at four injection locations ( $15^{\circ}\text{S}$ ,  $15^{\circ}\text{N}$ ,  $30^{\circ}\text{S}$ ,  $30^{\circ}\text{N}$ ) into one grid box at  $180^{\circ}$  longitude, and bounded by two  
152 pressure interfaces: 47.1 hPa and 39.3 hPa (approximate geometric altitude at gridbox midpoint of 21.6 km). The  
153 injection latitudes are the same as used in GLENS and in previous studies examining the model’s responses to  
154 single-point  $\text{SO}_2$  injections (Tilmes et al., 2017; Richter et al., 2017). These four injection locations are sufficient to  
155 independently control the targets that we are trying to achieve (Kravitz et al., 2017). This injection altitude is  
156 estimated to be achievable by existing aircraft technologies that could be adapted for climate intervention use  
157 (Bingaman et al., 2020).

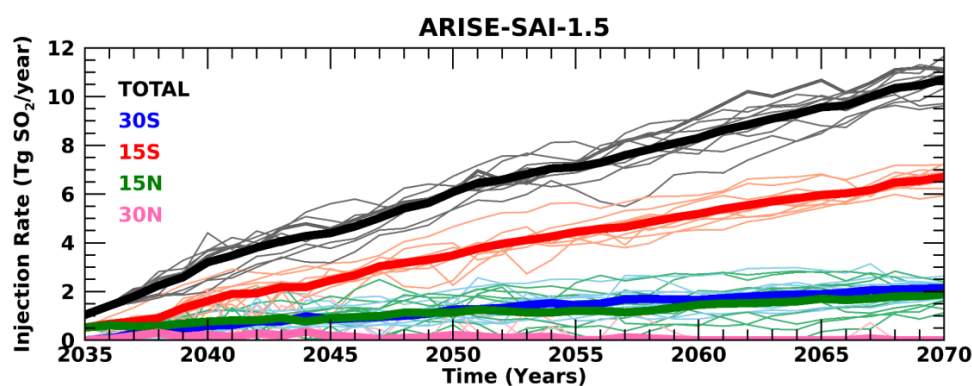
158 There is uncertainty among Earth system models with regard to when Earth’s global mean surface  
159 temperature ( $T_0$ ) will reach  $1.5^{\circ}\text{C}$  above pre-industrial levels. The recent Intergovernmental Panel of Climate  
160 Change (IPCC) Sixth Assessment Report (AR6) (IPCC, 2021) finds that  $1.5^{\circ}\text{C}$  over pre-industrial will very likely be  
161 exceeded in the near term (2021- 2040) under the very high greenhouse gas (GHG) emission scenario (SSP5-8.5)  
162 and likely to be exceeded under the intermediate and high GHG emissions scenarios (SSP2-4.5 and SSP3-7.0). The  
163 IPCC AR6 defines  $1.5^{\circ}\text{C}$  as the time at which  $T_0$  will reach  $0.65^{\circ}\text{C}$  above the historical reference period of 1995 -  
164 2014. The  $T_0$  between 1995 - 2014 is  $0.85^{\circ}\text{C}$  above the pre-industrial (PI) value defined as the 1850 - 1900 average  
165 in the observational record. Using 31 global models, Tebaldi et al. (2021) found that the average across models of  
166 when  $1.5^{\circ}\text{C}$  will be reached in 2028 under the SSP2-4.5 scenario (using 1995-2014 as  $0.84^{\circ}\text{C}$  rather than  $0.85^{\circ}\text{C}$   
167 above PI), but with considerable variation across models. The 20-year running average of  $T_0$  in CESM2(WACCM6)  
168 ( $T_0_{\text{CESM2}}$ ) relative to 1995 - 2014, reaches  $0.85^{\circ}\text{C}$  (or  $\sim 1.5^{\circ}\text{C}$  above PI  $T_0$ ) in 2029. To simplify future model  
169 intercomparisons, we choose the time period of 2020 - 2039 (or  $\sim 2030$  levels) as our reference period of when  
170  $T_0_{\text{CESM2}}$  is  $\sim 1.5^{\circ}\text{C}$  above PI values, and make that the target  $T_0$  in the climate intervention simulations. The year  
171 2035 was chosen as the beginning of intervention, since  $T_0_{\text{CESM2}}$  in every ensemble member of SSP2-4.5  
172 simulations is then consistently above the target temperature.

173 The amount of injection at each location is specified by a “controller” algorithm (MacMartin et al., 2014;  
174 Kravitz et al., 2017) that was used in GLENS and the simulations presented in Tilmes et al. (2020). After each year  
175 of simulation, the algorithm calculates the global mean temperature,  $T_0$ , north-south temperature gradient,  $T_1$ , and  
176 equator-to-pole temperature gradient,  $T_2$ , and based on the deviation from the goal, specifies the annual values of  
177 injections at the four locations for the subsequent year.  $T_1$  and  $T_2$  were defined in Kravitz et al. (2017), Equation 1.  
178 Based on the 2020 - 2039 mean of the SSP2-4.5 simulations with CESM2(WACCM6), the surface temperature  
179 targets for the ARISE-SAI-1.5 ensemble for  $T_0$ ,  $T_1$ , and  $T_2$  are 288.64 K, 0.8767 K, and  $-5.89$  K, respectively.



180 Simulations are carried out for 35 years (2035 - 2069), which is sufficient for us to consider both a transition period  
 181 of ~10 years and a quasi-equilibrium of at least 20 years after the controller converges. All simulations have  
 182 comprehensive monthly as well as high-frequency output for analysis of high-impact events (described in detail in  
 183 the Data Records section).

184 The first five members of ARISE-SAI-1.5 simulations were initialized in 2035 from the first five members  
 185 (001 to 005) of the SSP2-45 simulations carried out with CESM2(WACCM6); hence, all had different initial ocean,  
 186 sea-ice, land, and atmospheric initial conditions on January 1, 2035. Similarly to the SSP2-45 simulations,  
 187 subsequent ensemble members (006 through 010) were initialized from the same initial conditions as members 001  
 188 through 005, respectively, with an addition of a small temperature perturbation to the atmospheric initial condition  
 189 to create ensemble spread.



190  
 191 **Figure 1:** SO<sub>2</sub> injection rate as a function of time in ARISE-SAI-1.5 simulations at 30°S (blue), 15°S (red), 15°N  
 192 (green), 30°N (pink), and total (black). Thin lighter colored lines represent individual ensemble members, whereas  
 193 thick lines show the 10-member ensemble mean.  
 194

195 The amount of SO<sub>2</sub> injection in the ARISE-SAI-1.5 simulations chosen by the controller algorithm is  
 196 shown in Figure 1. The majority of SO<sub>2</sub> is injected at 15°S, with an approximate linear increase from 0.5 Tg SO<sub>2</sub> per  
 197 year in year 2035 to 6 Tg SO<sub>2</sub> per year in 2069. SO<sub>2</sub> injections at 30°S and 15°N are about 1/3 of that injected at 15°S.  
 198 Throughout all the ARISE-SAI-1.5 simulations, the amount of SO<sub>2</sub> injection at 30°N is very small, less than 0.5 Tg  
 199 SO<sub>2</sub> per year, diminishing to nearly zero by the end of the simulations. The distribution of SO<sub>2</sub> across the four  
 200 injection latitudes in ARISE-SAI-1.5 is very different from that in GLENS (Tilmes et al., 2018) despite having the  
 201 same goals for the controller. In GLENS, the majority of SO<sub>2</sub> was injected at 30°S and 30°N, with a significant  
 202 amount at 15°N, and almost none at 15°S; that is, GLENS required more injection in the Northern Hemisphere than  
 203 the Southern in order to maintain the interhemispheric temperature gradient T<sub>1</sub>, whereas ARISE-SAI-1.5 requires  
 204 more injection in the Southern Hemisphere to maintain T<sub>1</sub>. GLENS also required more at 30°N/30°S to maintain T<sub>2</sub>



205 than is required in ARISE-SAI-1.5. It is unclear at this time how much of this difference is a result of the different  
206 model version and how much is a result of changes in the forcing between RCP8.5 and SSP2-4.5.

## 207 **2.4 Output**

208 All model output for the simulations is based on community input and provided in NetCDF format. All variables are  
209 in time-series format, with one variable per file. 3-dimensional atmospheric output is on the original 70 model  
210 levels. Output consists of standard monthly mean CMIP6 output for the atmospheric, land, ocean, and sea-ice  
211 models. In addition, higher-frequency (daily averaged, 3-hourly averaged, 3-hourly instantaneous, and 1-hourly  
212 mean) output is available for the atmospheric model that will enable analysis of extreme events (e.g.: Tye et al.  
213 2022). The atmospheric output at various time frequencies is described in Appendix A, Tables A1 - A4. Daily  
214 averaged output of land model variables is shown in Tables A5 and A6, whereas 6-hourly output from the land  
215 model is listed in Table A7. Tables A8 and A9 show the daily output from the ocean and sea-ice models  
216 respectively. The table captions describe which output is specific to ARISE-SAI-1.5 and the new five SSP2-4.5  
217 CESM2(WACCM6) ensemble members, and which is common to all simulations. An online table showing all the  
218 output fields for the simulations, along with their description and units, is at:

219 <https://www.cgd.ucar.edu/ccr/strandwg/WACCM6-TSMLT-SSP245/>

220

## 221 **3 Results**

222 The intent of ARISE-SAI simulations is to provide the broader community a data set for examining various impacts  
223 of SCI on the multiple components of the Earth system. Below we present basic diagnostics that verify that the SO<sub>2</sub>  
224 injections and controller are working as intended, and we describe how well the temperature targets are being met.  
225 Detailed analysis of the simulations are left for future work.

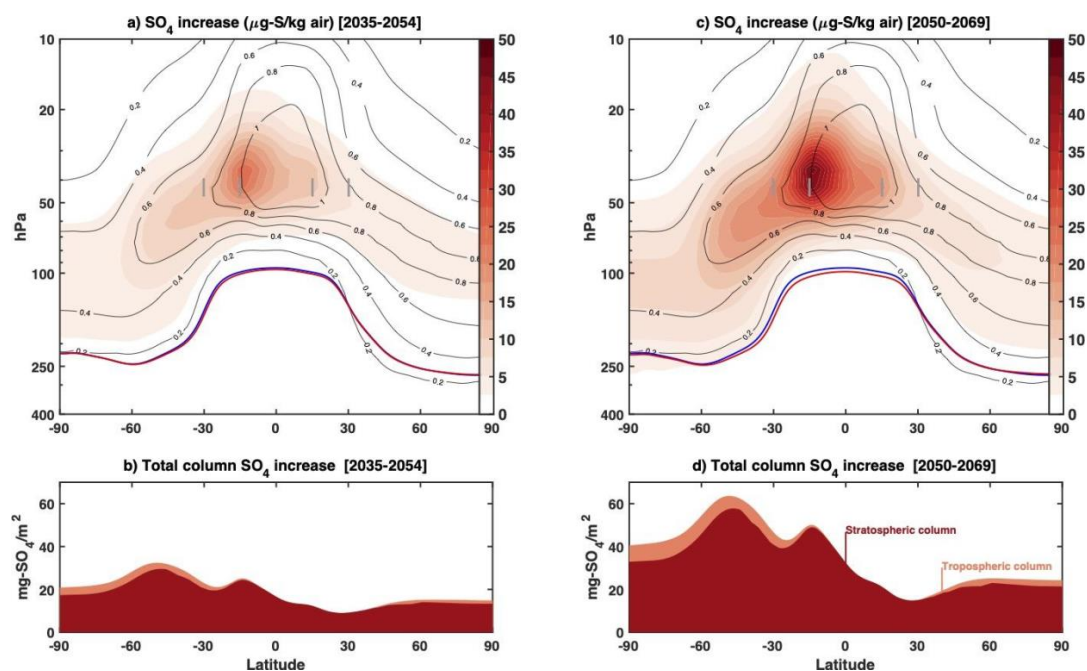
226

### 227 **3.1 Stratospheric Aerosols**

228 Injection of sulfur dioxide into the stratosphere results in the formation of sulfate aerosols, which are  
229 transported by the stratospheric Brewer-Dobson circulation (Andrews et al., 1987; Times et al., 2017). The  
230 dominance of SO<sub>2</sub> injections at 15°S in ARISE-SAI-1.5 results in a stratospheric sulfate (SO<sub>4</sub>) increase that  
231 primarily occurs in the southern hemisphere, with the majority of SO<sub>4</sub> concentrated near the primary injection  
232 location (Figure 2a, 2b). Averaged over the 2035 - 2054 period, there is a peak SO<sub>4</sub> increase of 25 mg-S/kg air (Fig  
233 2a) relative to the 2020 - 2039 mean, and averaged over 2050 - 2069an SO<sub>4</sub> increase of 48 mg-S/kg air is found near  
234 15°S, 40 hPa (Fig 2b). The zonally averaged latitudinal distribution of the increase in the column of SO<sub>4</sub> is shown in  
235 Figures 2c, d; both figures show the strong hemispheric asymmetry, and also a double peak at around 15°S and one  
236 near 50°S. The peak near 15°S is due to the predominant location of the injection, and matches the peak in  
237 concentration, the latter is due to the largest vertical stratospheric layer over which SO<sub>4</sub> is spread out (between 10  
238 and 22 km) compared to the layer in the tropical stratosphere (between 18 and 26 km). Integrated over 20 year  
239 periods of ARISE-SAI-1.5 simulations, there is little difference in the latitudinal distribution of column SO<sub>4</sub> between  
240 the various ensemble members, but amplitude differences of up to 15% exist (not shown), reflecting variability in  
241 the amount of SO<sub>2</sub> injection at each location and small differences in the stratospheric circulation.



242



243

244

245 **Figure 2:** Zonal mean stratospheric SO<sub>4</sub> concentration increase (in μg-S/kg of air) in (a) 2035-2054 and (c) 2050-  
 246 2069 relative to the 2020 - 2039 mean. Black contour lines show the background concentration in 2020-2039. Blue  
 247 line shows the annual mean tropopause height in the control period; the red line shows the annual mean tropopause  
 248 height in the ARISE simulation in 2035-2054 and 2050-2069, respectively. Gray shadings indicate the grid-boxes  
 249 where SO<sub>2</sub> is injected. Zonal mean total increase in the column burden of sulfate (in mg-SO<sub>4</sub>/m<sup>2</sup>) for (b) 2035 - 2054  
 250 and (d) 2050 - 2069. The contribution to the column increase is shown in dark red, for the fraction located in the  
 251 stratosphere, and in orange for the fraction located in the troposphere.

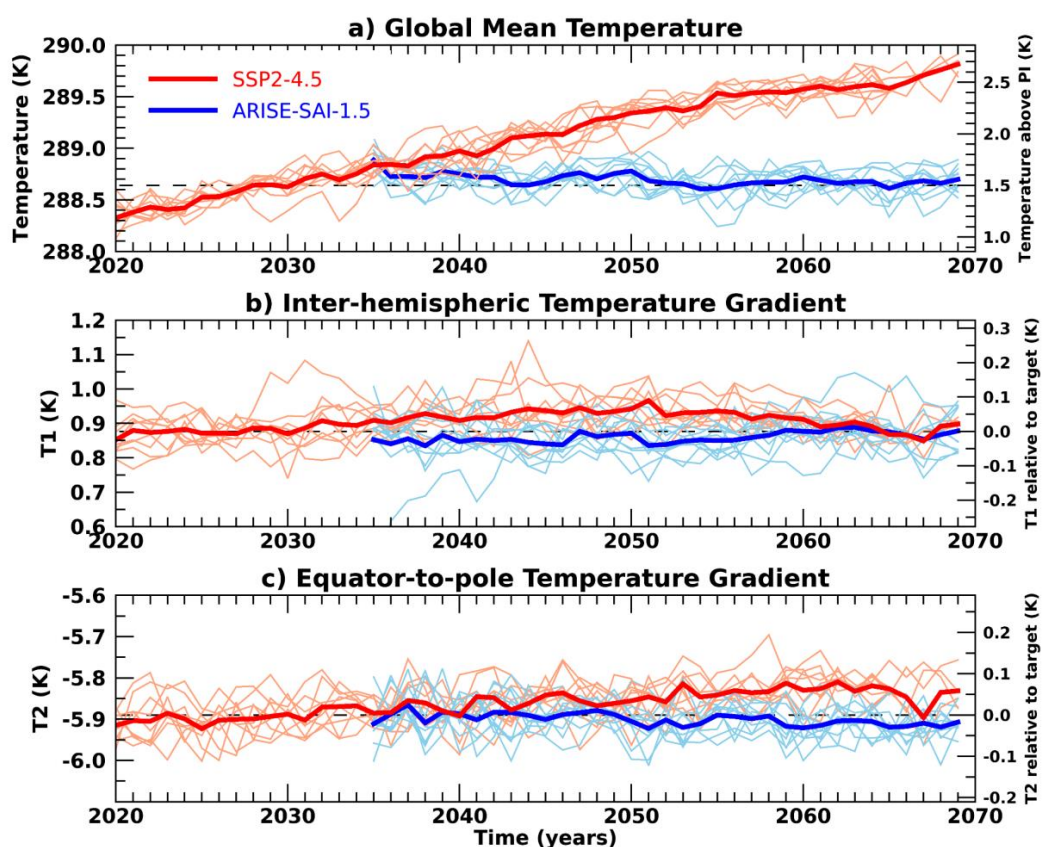
252

### 253 3.2 Meeting temperature targets

254 Global mean surface temperature, the inter-hemispheric temperature gradient, and equator-to-pole temperature  
 255 gradients for the SSP2-4.5 and ARISE-SAI-1.5 simulations are shown in Figure 3. There is a notable difference in  
 256 behavior of T1 and T2 in the SSP2-4.5 simulations as compared to the RCP8.5 simulations with CESM1(WACCM)  
 257 (not shown). In the CESM1(WACCM) simulations with RCP8.5, T1 and T2 were increasing steadily with time of  
 258 simulation, reaching a change in T1 of nearly 0.45 K, and a T2 change of 0.3 K by 2070 relative to ~ 2020 - 2039  
 259 mean (Tilmes et al. 2018). In contrast, T1 and T2 in the SSP2-4.5 simulation are increasing much more slowly, less  
 260 than 0.05 K for T1 and less than 0.1 K for T2 between the reference period (2020-2039) and 2070. The more  
 261 moderate (SSP2-4.5) emission scenario used in the CESM2(WACCM6) control simulations partially explains the  
 262 slower increase of T1 and T2 with time, however not all. Simulations with CESM2(WACCM6) and SSP5-8.5  
 263 scenarios also show a much slower increase of T1 and T2 as compared to CESM1(WACCM) with RCP8.5.



264 Differing modeling physics, in particular cloud feedbacks, between CESM1 and CESM2 are most likely responsible  
 265 for the differences in projected spatial patterns of surface warming between the two model configurations, as well as  
 266 changes in the Atlantic Meridional Overturning Circulation as discussed in Tilmes et al. (2019). Simulations with  
 267 CESM2 and RCP emissions are currently in production to understand the relative role of differences in forcing and  
 268 differences in model physics on projected spatial patterns of global mean temperature and other variables between  
 269 CESM1 and CESM2.  
 270



271  
 272 **Figure 3:** Global mean a) surface temperature, b) inter-hemispheric temperature gradient, T1, and c) equator-to-pole  
 273 temperature gradient, T2, for SSP2-4.5 (red) and ARISE-SAI-1.5 (blue) simulations. Thin lines represent individual  
 274 ensemble members, whereas the thick lines show the ensemble mean.

275  
 276 The differences between the projected surface temperature patterns in CESM2 as compared to CESM1  
 277 have implications for climate intervention. Since the changes in T1 and T2 targets differ between the  
 278 CESM1(WACCM) and CESM2(WACCM6) future simulations, the controller selects different SO<sub>2</sub> injection  
 279 locations to best counteract these changes. Injections needed to offset increasing T1 and T2 in CESM1(WACCM)

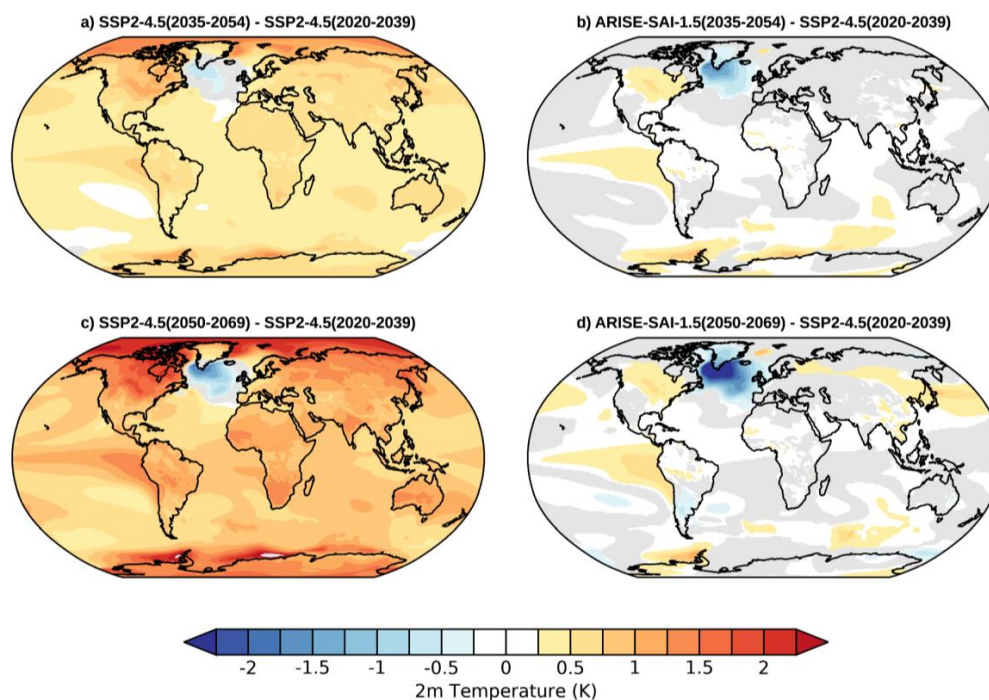


280 required primarily injections at 30°S and 30°N, whereas a small change in T1 and T2 relative to the 2020 - 2039  
 281 period in CESM2(WACCM6), SSP2-4.5 requires injections primarily at 30°S. The SO<sub>2</sub> injections applied in ARISE-  
 282 SAI-1.5 do a very good job at keeping the global mean temperature, T1 and T2 at the target levels. This is  
 283 demonstrated by the blue lines in Figure 2. There is a fair amount of variability among the individual ensemble  
 284 members (thin light blue lines) in their ability to meet the global mean, T1 and T2 targets, however the ensemble  
 285 mean (thick blue line) shows very good agreement between these variables and their target values.

286

287 **3.3 Surface temperature and precipitation**

288



289

290 **Figure 4:** Ensemble and annual mean surface (2m) temperature differences between a) SSP2-4.5 (2035-2054) and  
 291 SSP2-4.5 (2020-2039), b) ARISE-SAI-1.5 (2035-2054) and SSP2-4.5 (2020-2039), c) SSP2-4.5 (2050-2069) and  
 292 SSP2-4.5 (2020-2039), and d) ARISE-SAI-1.5 (2050-2069) and SSP2-4.5 (2020-2039). Gray shading indicates  
 293 regions where the differences are not statistically significant at the 95% level using a two-sided Student's t test.

294

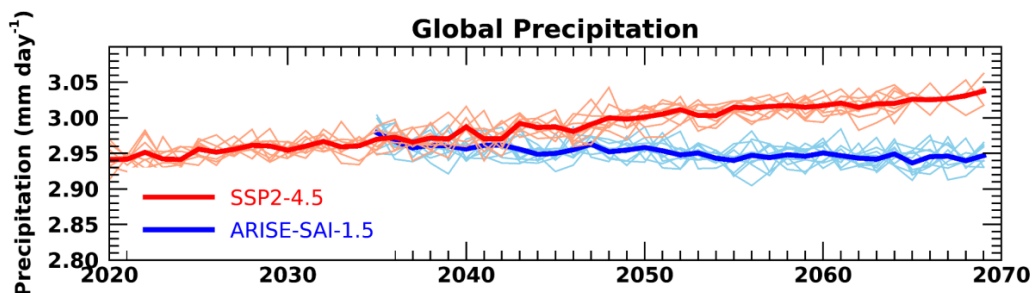
295 Figure 4 shows the ensemble and annual mean surface temperature changes for two time periods, 2035 - 2054 and  
 296 2050 - 2069, during the SSP2-4.5 and ARISE-SAI-1.5 simulations relative to the 2020 - 2039 period. Fig 4 a, c  
 297 show the steady increase in surface temperature with time over the majority of the globe, with largest warming  
 298 occurring in the Northern Hemisphere high latitudes. The North Atlantic is the only region of the globe that is



299 cooling in the 21st century. This “warming hole” in the North Atlantic is a feature of several of the recent generation  
 300 Earth system models and is attributed to the AMOC (Drijfhout et al. 2012, Chemke et al. 2020, Keil et al. 2020).  
 301 Specifically, in a warming climate with a reduction in the deep water formation, the AMOC weakens. This results in  
 302 less heat transport into the Northern North Atlantic, producing cooler temperatures that oppose the anticipated  
 303 effects of global warming. Figures 4b and 4d demonstrate the success of the SAI strategy in keeping the global  
 304 temperatures near the 2020 - 2039 average, or at ~ 1.5 K above pre-industrial values. In ARISE-SAI-1.5, near  
 305 surface annual mean temperature throughout the entire simulation is within 0.5 K of that goal over the majority of  
 306 the globe. The largest exception to that is the North Atlantic warming hole, where surface temperatures remain  
 307 cooler relative to the northern North Atlantic than in the present day or with comparison to SSP2-4.5. In addition, in  
 308 the ensemble mean, ARISE-SAI-1.5 simulations show residual warming over North America, as well as over  
 309 Eastern South Pacific Ocean (off the coast of South America), and in parts of Antarctica as compared to the 2020 -  
 310 2039 period. Residual changes relative to the target period from the application of SAI are expected, as SAI can not  
 311 perfectly reverse the effects of increasing greenhouse gases.

312 The precipitation changes in SSP2-4.5 and ARISE-SAI-1.5 simulations for the same time periods  
 313 examined for surface temperature changes are shown in Figures 5 and 6. Consistent with prior similar studies, SSP2-  
 314 4.5 simulations show primarily an increase of precipitation in a warming climate, with the largest increases along the  
 315 Equatorial Pacific Ocean, and a strong drying region northward of that (Figs 5, 6a,c). In ARISE-SAI-1.5, consistent  
 316 with previous studies (Kravitz et al., 2017; Lee et al. 2020), restoring global mean temperature is associated with an  
 317 overall decrease in annual mean precipitation (Fig 5), however regionally both increases and decreases occur. In  
 318 ARISE-SAI-1.5, the increased precipitation across the Equatorial Pacific seen in SSP2-4.5 decreases in magnitude,  
 319 but is still a persistent feature. ARISE-SAI-1.5 also shows drying north and south of that region as well as  
 320 intensified drying over Northern South America, South Africa, Indian Ocean south of the Equator and northernmost  
 321 Australia. The Indian Ocean north of the Equator and India are projected to be wetter in ARISE-SAI-1.5 as  
 322 compared to the 2020 - 2039 period of SSP2-4.5.

323

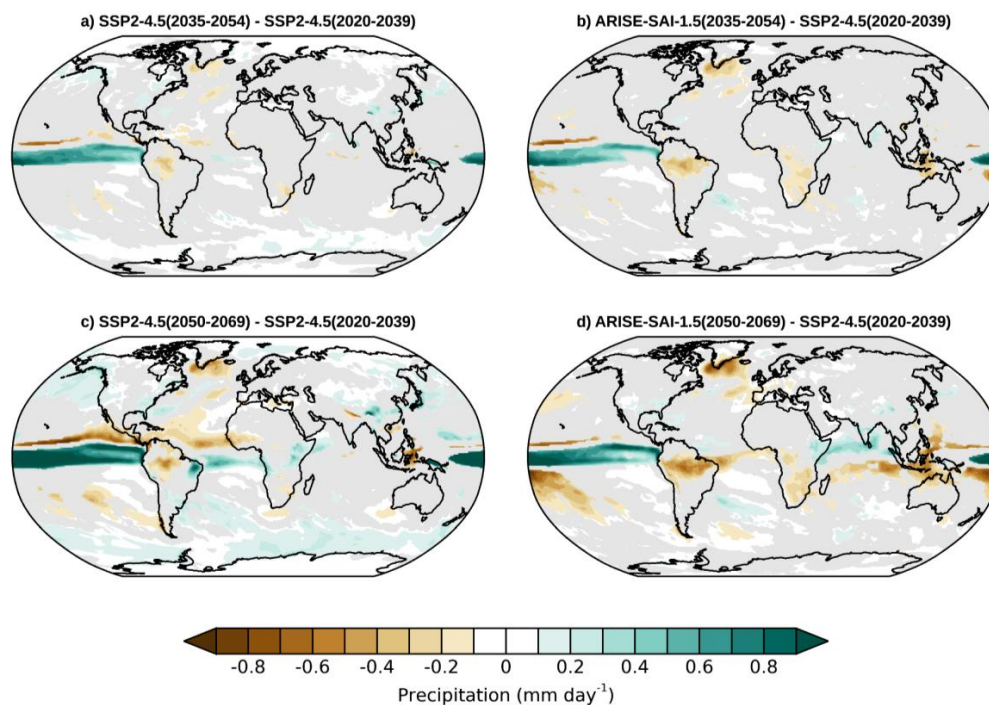


324

325

Figure 5: Same as Figure 3a but for precipitation.

326



327

328 **Figure 6:** Same as Figure 4 but for annual mean precipitation.

329

#### 330 **4 Conclusions**

331 We have described here a detailed new modeling protocol and first set of simulations entitled Assessing Responses  
332 and Impacts of Solar climate intervention on the Earth system with Stratospheric Aerosol Injection (ARISE-SAI),  
333 for studies of impacts of climate intervention using stratospheric aerosols. We have carried out these simulations  
334 utilizing CESM2(WACCM6) and provided extensive output for community analysis. The protocol for simulations  
335 described here can be easily implemented in other Earth system models with similar capabilities; furthermore, the  
336 protocol can easily be adapted to explore different climate intervention scenarios considering other climate targets,  
337 such as different global mean cooling targets, and in the future extended to other types of climate intervention, such  
338 as marine cloud brightening. The SAI injection strategy builds on the approach used in GLENS that was carried out  
339 with CESM1(WACCM), but uses a more moderate background emissions scenario, a start date of 2035 rather than  
340 2020, and a target temperature of 1.5°C over pre-industrial following the AR6 definition; the set of simulations  
341 presented here also uses a newer version of CESM, which is the same as used for CMIP6 (Gettelman et al., 2019). In  
342 these new simulations, the SO<sub>2</sub> injections required to keep the global mean temperature, interhemispheric  
343 temperature gradient, and pole-to-pole temperature gradient at the target level in ARISE-SAI-1.5 are needed  
344 primarily at 15°S, in contrast to GLENS which utilized SO<sub>2</sub> injections primarily at 30°N and 30°S. The reasons for  
345 these differences are currently being investigated in detail, and it highlights the need to reproduce such experiments



346 with other climate models to understand their sources. Surface climate in ARISE-SAI-1.5 is very similar to that  
 347 during the reference period (2020 - 2039), however residual changes still remain, in particular in the North Atlantic,  
 348 where surface temperature is cooler than in the reference period. The robustness of these projected regional residuals  
 349 in other climate models, or under different climate targets, would also be of extreme interest. Consistent with prior  
 350 studies, global mean precipitation in ARISE-SAI-1.5 is smaller than during the reference period.

351

352 **Appendix A**

353

Variable Name	Description
ACTNL	Average Cloud Top droplet number
ACTREL	Average Cloud Top droplet effective radius
bc_a4_SRF*	Black carbon in additional mode in bottom layer
BURDENBCdn	Black carbon aerosol burden, day night
BURDENDUSTdn	Dust aerosol burden, day night
BURDENPOMdn	Particulate organic matter aerosol burden, day night
BURDENSEASALTdn	Seasalt aerosol burden, day night
BURDENSO4dn	Sulfate aerosol burden, day night
BURDENSOAdn	SOA aerosol burden, day night
BUTGWSPEC	Zonal wind tendency from convective gravity waves
CDNUMC	Vertically-integrated droplet concentration
CLDICE	Grid box averaged cloud ice amount
CLDLIQ	Grid box averaged cloud liquid amount
CLDTOT	Vertically-integrated total cloud
CLOUD	Cloud fraction
CMFMC	Moist convection (deep+shallow) mass flux
CMFMCZM	Convection mass flux from ZM deep
dst_a1*	Dust concentration in accumulation mode
dst_a2*	Dust concentration in Aitken mode
dst_a3*	Dust concentration in coarse mode
dst_a2_SRF*	Aitken mode dust in bottom layer



FCTL	Fractional occurrence of cloud top liquid
FLDS	Downwelling longwave flux at surface
FLDSC	Clearsky Downwelling longwave flux at surface
FLNR	Net longwave flux at tropopause
FLNS	Net longwave flux at surface
FLNSC	Clearsky net longwave flux at surface
FLNT	Net longwave flux at top of model
FLNTC	Clearsky net longwave flux at top of model
FLUT	Upwelling longwave flux at top of model
FLUTC	Clearsky upwelling longwave flux at top of model
FSDS	Downwelling solar flux at surface
FSDSC	Clearsky downwelling solar flux at surface
FSNR	Net solar flux at tropopause
FSNS	Net solar flux at surface
FSNSC	Clearsky net solar flux at surface
FSNTOA	Net solar flux at top of atmosphere
FSNTOAC	Clearsky net solar flux at top of atmosphere
LHFLX	Surface latent heat flux
MASS	mass of grid box
O3	Ozone
MSKtem	Transformed Eulerian Mean diagnostics mask
OMEGA	Vertical velocity (pressure)
OMEGA500	Vertical velocity at 500 hPa
PBLH	Planetary boundary layer height
PDELDRY	Dry pressure difference between levels
PHIS	Surface geopotential
PM25_SRF	PM2.5 in the bottom layer
pom_a4_SRF*	Particulate organic matter in additional mode in bottom layer



PRECC	Convective precipitation rate
PRECT	Total (convective and large-scale) precipitation rate
PRECTMX	Maximum (convective and large-scale) precipitation rate
PS	Surface pressure
PSL	Sea level pressure
Q	Specific humidity
QREFHT	Reference height humidity
QSNOW	Diagnostic grid-mean snow mixing ratio
RELHUM	Relative humidity
RHREFHT	Reference height relative humidity
SFso4_a1*	surface flux of SO <sub>4</sub> in accumulation mode
SFso4_a2*	surface flux of SO <sub>4</sub> in Aitken mode
SFbc_a4*	Surface flux of black carbon in additional mode
SFpom_a4*	Particulate organic matter in additional mode
SFdst_a1*	Surface flux of dust in accumulation mode
SFdst_a2*	Surface flux of dust in Aitken mode
SFdst_a3*	Surface flux of dust in coarse mode
SHFLX	Surface sensible heat flux
SO2	Sulfur dioxide concentration
SOLIN	Solar insolation
SOLL	Solar downward near infrared diffuse to surface
SOLSD	Solar downward visible diffuse to surface
T	Temperature
T500, T700, T850	Temperature at 500, 700 and 850 hPa respectively
TAUBLJX	Zonal integrated drag from Beljaars SGO
TAUBLJY	Meridional integrated drag from Beljaars SGO
TAUGWX	Zonal gravity wave surface stress
TAUGWY	Meridional gravity wave surface stress



TAUX	Zonal surface stress
TAUY	Meridional surface stress
TGCLDIWP	Total grid-box cloud ice water path
THzm	Zonal-Mean potential temperature defined on ilevels
TGCLDLWP	Total grid-box cloud liquid water path
TMQ	Total (vertically integrated) precipitable water
TREFHT	Reference height temperature
TREFHTMN**	Minimum reference height temperature
TREFHTMX**	Maximum reference height temperature
TS	Surface temperature (radiative)
TSMN	Minimum surface temperature
TSMX	Minimum surface temperature
U	Zonal wind
U10	10m wind speed
UTGWORO	U tendency - orographic gravity wave drag
UTGWSPEC	U tendency - non-orographic gravity wave drag
UVzm	Meridional flux of zonal momentum: 3D zonal mean
UWzm	Vertical flux of zonal momentum: 3D zonal mean
Uzm	Zonal mean zonal wind defined on ilevels
V	Meridional wind
VTHzm	Meridional Heat Flux: 3D zonal mean
Vzm	Zonal mean meridional wind defined on ilevels
Wzm	Zonal mean vertical wind defined on ilevels
Z3	Geopotential Height (above sea level)
Z500	Geopotential height at 500 hPa pressure surface
SO2	SO <sub>2</sub> concentration

354

355

356

**Table A1:** Available daily averaged output from the atmospheric model in ARISE-SAI-1.5 simulations and SSP2-4.5 CESM2(WACCM6) simulations. Variables marked with a '\*\*' are not available from the first five members of



357 CESM2(WACCM6) SSP2-4.5 simulations. \*\*indicates variables that are available (but erroneous) in the first five  
 358 members of CESM2(WACCM6) SSP2-4.5 simulations.  
 359

Name of Variable(s)	Variable Description
CAPE	Convective available potential energy
CIN	Convective inhibition
CLDLow	Vertically-integrated low cloud
FLUT	Upwelling longwave flux at top of model
PRECT	Total (convective and large-scale) precipitation rate
PRECC	Convective precipitation rate
PRECSC	Convective snow rate (water equivalent)
PRECSL	Large-scale snow rate (water equivalent)
PSL	Sea level pressure
Q200, Q500, Q700, Q850, Q925	Specific humidity at 200, 500, 700, 850 and 925 hPa respectively
T200, T300, T500, T700, T850, T925	Temperature at 200, 300, 500, 700, 850 and 925 hPa respectively
TMQ	Total (vertically integrated) precipitable water
U200, U300, U500, U700, U850, U925	Zonal wind at 200, 300, 500, 700, 850 and 925 hPa respectively
V200, V300, V500, V700, V850, V925	Meridional wind at 200, 300, 500, 700, 850 and 925 hPa respectively
Z200, Z500, Z700, Z850, Z925	Geopotential height at 200, 500, 700, 850 and 925 hPa respectively

360  
 361 **Table A2:** 3-hourly averaged output from the atmospheric model in ARISE-SAI-1.5 simulations and additional five  
 362 SSP2-4.5 CESM2(WACCM6) simulations. None of the above output is contained in the first five ensemble  
 363 members of CESM2(WACCM6) SSP2-4.5 simulations.  
 364  
 365



366

IVT	Integrated water vapor transport
PS	Surface Pressure
Q*	Specific humidity
T*	Temperature
TS	Surface temperature (radiative)
PSL	Sea level pressure
RELHUM*	Relative humidity
TMQ	Total (vertically integrated) precipitable water
U*	Zonal wind
U10	10m wind speed
uIVT	Zonal water vapor transport
vIVT	Meridional water vapor transport
V*	Meridional wind
Z3*	Geopotential Height

367

368 **Table A3:** 3-hourly instantaneous output from the atmospheric model in ARISE-SAI-1.5 simulations and additional  
 369 five SSP2-4.5 CESM2(WACCM6) simulations. For the variables marked with a ‘\*’, only the bottom-most 22 levels  
 370 were retained, hence levels for those variables range from 1000 to 103 hPa. None of the above output is contained in  
 371 the first five ensemble members of CESM2(WACCM6) SSP2-4.5 simulations.

372



373

374

Name of Variable	Variable Description
NO2_SRF	NO2 in bottom layer
O3_SRF	O3 in bottom layer
PM25_SRF	PM2.5 at the surface
PRECC	Convective precipitation rate
PRECT	Total (convective and large-scale) precipitation rate
TS	Surface temperature (radiative)

375

376 **Table A4:** 1-hourly instantaneous output from the atmospheric model in ARISE-SAI-1.5 simulations and additional

377 five SSP2-4.5 CESM2(WACCM6) simulations. None of the above output is contained in the first five ensemble

378 members of CESM2(WACCM6) SSP2-4.5 simulations.

379

380

381

382

Variable Name	Description
AR	Autotrophic respiration
COL_FIRE_CLOSS	Total column-level fire C loss
CPHASE	Crop phenology phase
DSTDEP	Total dust deposition
DSTFLXT	Total surface dust emission
DWT_CONV_CFLUX_PATCH	Patch-level conversion C flux
DWT_SLASH_CFLUX	Slash C flux to litter and CWD due to land use
DWT_WOOD_PROD_UCTC_GAIN_PATCH	Patch-level landcover change-driven addition to wood product pools
EFLX_LH_TOT	Total latent heat flux
FGR	Heat flux into soil/snow including snow melt and lake / snow light transmission
FIRA	Net infrared (longwave) radiation



FIRE	Emitted infrared (longwave) radiation
FROOTC	Fine root carbon
FSH	Sensible heat not including correction for land use change and rain/snow conversion
FSR	Reflected solar radiation
GDDHARV	Growing degree days needed to harvest
GDDPLANT	Accumulated growing degree days past planting date for crop
GPP	Gross primary production
GRAINC_TO_FOOD	Grain carbon to food
H2OSNO	Snow depth (liquid water)
HR	Total heterotrophic respiration
HTOP	Canopy top
NPP	Net primary production
Q2M	2m specific humidity
QDRAI	Sub-surface drainage
QDRAI_XS	Saturation excess drainage
QIRRIG	Water added through irrigation
QOVER	Surface runoff
QRUNOFF	Total liquid runoff
QSNOMELT	Snow melt rate
QSOIL	Ground evaporation
QTOPSOIL	Water input to surface
QVEGE	Canopy evaporation
QVEGT	Canopy transpiration
RH2M	2m relative humidity
SLASH_HARVESTC	Slash harvest carbon
SNOWDP	Gridcell mean snow height
SOILWATER_10CM	Soil liquid water + ice in top 10cm of soil
TG	Ground temperature



TLAI	Total projected leaf area index
TOTSOILLICE	Vertically summed soil ice
TOTSOILLIQ	Vertically summed soil liquid water
TREFMNAV	Daily minimum of average 2-m temperature
TREFMXAV	Daily maximum of average 2-m temperature
TSA	2m air temperature
TSKIN	Skin temperature
TSOI_10CM	Soil temperature in top 10cm of soil
TV	Vegetation temperature
TWS	Total water storage
U10	10-m wind
U10_DUST	10-m wind for dust model
URBAN_HEAT	Urban heating flux
WASTEHEAT	Sensible heat flux from heating/cooling sources of urban waste heat
WOOD_HARVESTC	Wood harvest carbon

383

384 **Table A5:** Available daily averaged output from the land model at landunit-level in ARISE-SAI-1.5 simulations and

385 additional five SSP2-4.5 CESM2(WACCM6) simulations. None of the above output is contained in the first five

386 ensemble members of CESM2(WACCM6) SSP2-4.5 simulations.

387

CPHASE	Crop phenology phase
CROPPROD1C	1-yr grain product carbon
CWDC_vr	Coarse woody debris carbon, vertically resolved)
CWDN_vr	Coarse woody debris nitrogen (vertically resolved)
EFLX_LH_TOT	Total latent heat flux
FGR	Heat flux into soil/snow including snow melt and lake / snow light transmission
FPSN	Photosynthesis
FROOTC	Fine root carbon
FSH	Sensible heat not including correction for land use change and



	rain/snow conversion
FSNO_ICE	Fraction of ground covered by snow
GDDHARV	Growing degree days needed to harvest
GDDPLANT	Accumulated growing degree days past planting date for crop
GPP	Gross primary production
GRAINC	Grain carbon
H2OSOI	Volumetric soil water
HTOP	Canopy top
LEAFC	Leaf carbon
LEAFN	Leaf Nitrogen
LITR1C_vr, LITR2C_vr, LITR3C_vr	Amount of carbon in litter in different decomposition pools, vertically resolved
LITR1N_vr, LITR2N_vr, LITR3N_vr	Amount of nitrogen in litter in different decomposition pools, vertically resolved
LIVESTEMC	Live stem carbon
PCT_CFT	% of each crop on the crop landunit
PCT_GLC_MEC	% of each GLC elevation class on the glc_mec landunit
PCT_LANDUNIT	% of each landunit on grid cell
PCT_NAT_PFT	% of each PFT on the natural vegetation (i.e., soil) landunit
QICE_FORC	Surface mass balance of glaciated grid cells forcing sent to the glacier model
QIRRIG	Water added through irrigation
RAIN	Atmospheric rain, after rain/snow repartitioning based on temperature
Rnet	Net radiation
SMINN	Soil mineral N
SMP	Soil matric potential
SOILC_vr	SOIL C (vertically resolved)
SOILN_vr	SOIL N (vertically resolved)



TLAI	Total projected leaf area index
TOPO_FORC	Topographic height sent to glacier model
TOTLITC	Total litter carbon
TOTSOMC	Total soil organic matter carbon
TOTVEGC	Total vegetation carbon, excluding cpool
TOT_WOODPRODC	Total wood product carbon
TREFMNAV	Daily minimum of average 2-m temperature
TREFMXAV	Daily maximum of average 2-m temperature
TSA	2m air temperature
TSAI	Skin temperature
TSRF_FORC	Surface temperature sent to glacier model
TV	Vegetation temperature

388

389

390

391

392

**Table A6:** Available daily averaged output from the land model at gridcell-level in ARISE-SAI-1.5 simulations and additional five SSP2-4.5 CESM2(WACCM6) simulations. None of the above output is contained in the first five ensemble members of CESM2(WACCM6) SSP2-4.5 simulations.



393

Name of Variable	Variable Description
EFLX_LH_TOT	Total latent heat flux
FSH	Sensible heat not including correction for land use change and rain/snow conversion
H2OSNO	Snow depth (liquid water)
H2OSOI	Volumetric soil water
QDRAI	Sub-surface drainage
QDRAI_XS	Saturation excess drainage
QOVER	Surface runoff
QRUNOFF	Total liquid runoff
QSNOMELT	Snow melt rate
QSOIL	Ground evaporation
QTOPSOIL	Water input to surface
QVEGE	Canopy evaporation
QVEGT	Canopy transpiration
SOILICE	Soil ice
SOILLIQ	Soil liquid water
SOILWATER_10CM	Soil liquid water and ice in top 10cm of soil
TOTSOILICE	Vertically summed soil cice
TOTSOILLIQ	Vertically summed soil liquid water
TWS	Total water storage

394

395

396 **Table A7:** 6-hourly averaged output from the land model in ARISE-SAI-1.5 simulations and additional five SSP2-

397 4.5 CESM2(WACCM6) simulations. None of the above output is contained in the first five ensemble members of

398 CESM2(WACCM6) SSP2-4.5 simulations.

399

400

401

402

403



404  
405  
406  
407  
408

Name of Variable	Variable Description
CaCO3_form_zint_2	Total CaCO3 formation vertical integral
diatChl_SURF	Diatom chlorophyll surface value
diatC_zint_100m	Diatom carbon 0-100m vertical integral
diazChl_SURF	Diazotroph chlorophyll surface value
diazC_zint_100m	Diazotroph carbon 0-100m vertical integral
DpCO2_2	Atmosphere-ocean difference in the partial pressure of CO2
ECOSYS_IFRAC_2	Ice fraction for ecosystem fluxes
ECOSYS_XKW_2	Gas transfer velocity computed based on wind speed squared for ecosys fluxes
FG_CO2_2	Dissolved inorganic carbon surface gas glux
photoC_diat_zint_2	Diatom carbon fixation vertical integral
photoC_diaz_zint_2	Diazotroph carbon fixation vertical integral
photoC_sp_zint_2	Diatom carbon fixation vertical integral
spCaCO3_zint_100m	Small Phyto CaCO3 0-100m vertical integral
spChl_SURF	Small phyto chlorophyll surface value
spC_zint_100m	Small phyto carbon 0-100m vertical integral
STF_O2_2	Dissolved oxygen surface flux
zooC_zint_100m	Zooplankton carbon 0-100m vertical integral
HMXL_DR_2	Mixed-Layer depth
SSS	Sea surface salinity
SST	Surface potential temperature
SST2	Surface potential temperature**2
XMXL_2	Diazotroph carbon fixation vertical integral

409  
410  
411

**Table A8:** Daily averaged output from the ocean model in ARISE-SAI-1.5 simulations and all SSP2-4.5 CESM2(WACCM6) simulations.



412

413

414

Name of Variable	Variable Description
aice_d	cce area (aggregate)
aicen_d	ice area, categories
apond_ai_d	melt pond fraction of grid cell
congel_d	congelation ice growth
daidtd_d	area tendency dynamics
daidtt_d	area tendency thermodynamics
dvidtd_d	volume tendency dynamics
dvidtt_d	volume tendency thermodynamics
frazil_d	frazil ice growth
fswabs_d	snow/ice/ocn absorbed solar flux
fswdn_d	down solar flux
fswthru_d	shortwave through the sea ice to ocean
hi_d	grid cell mean ice thickness
hs_d	grid cell mean snow thickness
ice_present_d	fraction of time-avg interval that ice is present
meltb_d	basal ice melt
meltl_d	lateral ice melt
melts_d	top snow melt
meltt_d	top ice melt
sisnthick_d	sea ice snow thickness
sispeed_d	ice speed
sitemptop_d	sea ice surface temperature
sithick_d	sea ice thickness
siu_d	ice x velocity component
siv_d	ice y velocity component



vicen_d	ice volume, categories
vsnon_d	snow depth on ice, categories

415

416 **Table A9:** Daily averaged output from the sea-ice model in ARISE-SAI-1.5 simulations and all SSP2-4.5  
 417 CESM2(WACCM6) simulations.

418

419 **Code Availability**

420

421 CESM2(WACCM6) is freely available from <https://www.cesm.ucar.edu/>. CESM tag cesm2.1.4-rc.08 was used to  
 422 carry out the simulations. Python scripts to generate the case directories with appropriate model tags and output can  
 423 be found at <https://zenodo.org/record/6474201>. The code for the SO<sub>2</sub> injections controller can be downloaded from  
 424 <https://zenodo.org/record/6471092#.Y176rPPMKQc>.

425

426

427 **Data Availability**

428 All the data presented in this manuscript are available at <https://zenodo.org/record/6473954#.YmCAwy-B3qA>  
 429 from the CESM2(WACCM6) SSP2-4.5 simulations and at <https://zenodo.org/record/6473775#.YmCAy-B3qA>  
 430 from the ARISE-SAI-1.5 simulations. Complete output from all 10 members of CESM2(WACCM6) SSP2-4.5  
 431 simulations and ARISE-SAI-1.5 simulations is freely available the NCAR Climate Data Gateway at  
 432 <https://doi.org/10.26024/0cs0-ev98> and <https://doi.org/10.5065/9kcn-9y79> respectively. We anticipate community  
 433 analysis of various aspects of the Earth system of the ARISE-SAI-1.5 simulations. There is no obligation to inform  
 434 the project lead about the analysis you are performing, but it would be helpful in order to coordinate analysis and  
 435 avoid duplicate efforts.

436

437 **Author contribution**

438 JR designed and carried out simulations, compiled output requests, created most of the figures, and drafted the  
 439 manuscript. DV set-up the injection controller, carried out simulations, created a figure, and wrote parts of the  
 440 manuscript. DM co-designed the simulations and helped with interpretation of results. DB created the time series of  
 441 and archived all the data. NR created namelists with desired output and scripts to easily set-up the simulations. WL  
 442 analyzed the control simulations and provided targets for the controller. MT and JL gave input to simulation design  
 443 and data output requests. All authors reviewed the manuscript.

444

445 **Competing interests**

446 The authors declare that they have no conflict of interest.

447

448 **Acknowledgements**



449 This material is based upon work supported by the National Center for Atmospheric Research, which is a major  
450 facility sponsored by the National Science Foundation under Cooperative Agreement no. 1852977 and by  
451 SilverLining through its Safe Climate Research Initiative. The Community Earth System Model (CESM) project is  
452 supported primarily by the National Science Foundation. Computing and data storage resources, including the  
453 Cheyenne supercomputer (doi:10.5065/D6RX99HX), were provided by the Computational and Information Systems  
454 Laboratory (CISL) at NCAR.

455

#### 456 **References**

457 Andrews, D. G., Holton, J. R., and Leovy, C. B.: Middle atmosphere dynamics. San Diego, CA: Academic Press.,  
458 1987.

459 Beljaars, A. C. M., Brown, A. R., and Wood, N.: A new parameterization of turbulent orographic form drag.  
460 Quarterly Journal of the Royal Meteorological Society, 130, 1327–1347. <https://doi.org/10.1256/qj.03.73>,  
461 2004.

462 Burgess, M. G., J. Ritchie, J. Shapland and Pielke R. Jr.: IPCC baseline scenarios have over-projected CO2  
463 emissions and economic growth. *Env. Res. Lett.*, 16, 014016, <https://doi.org/10.1088/1748-9326/abcd2>,  
464 2021.

465 Carlson, C. J., and Trisos, C. H.: Climate engineering needs a clean bill of health. *Nature Climate Change*, 8(10),  
466 843–845, <https://doi.org/10.1038/s41558-018-0294-7>, 2018.

467 Chemke, R., Zanna, L., and Polvani, L. M.: Identifying a human signal in the North Atlantic warming hole. *Nature*  
468 *Communications*, 11(1), 1–7, 2022.

469 Coburn, J., and Pryor, S. C.: Differential Credibility of Climate Modes in CMIP6. *J. Climate*, 34(20), 8145-8164,  
470 2021.

471 Bingaman D. C, Christian V. Rice, Wake Smith and Patrick Vogel: A Stratospheric Aerosol Injection Lofter  
472 Aircraft Concept: Brimstone Angel, AIAA 2020-0618, AIAA Scitech 2020 Forum, January 2020.

473 Danabasoglu, G., Bates, S. C., Briegleb, B. P., Jayne, S. R., Jochum, M., Large, W. G., Peacock S., Yeager S. G.:  
474 The CCSM4 ocean component. *Journal of Climate*, 25, 1361–1389. [https://doi.org/10.1175/JCLI-D-11-](https://doi.org/10.1175/JCLI-D-11-00091.1)  
475 [00091.1](https://doi.org/10.1175/JCLI-D-11-00091.1), 2012.

476 Danabasoglu, G., Lamarque, J.-F., Bacmeister, J., Bailey, D. A., DuVivier, A. K., Edwards, J., Emmons L. K.,  
477 Fasullo J., Garcia R., Gettelman A., Hannay C., Holland M. M., Large W. G., Lauritzen P. H., Lawrence D.  
478 M., Lenaerts J. T. M., Lindsay K., Lipscomb, W. H., Mills, M. J., Neale R., Oleson K. W., Otto-Bliesner



- 479 B., Phillips A. S., Sacks W., Tilmes S., van Kampenhout L., Vertenstein M., Bertini A., Dennis J., Deser  
480 C., Fischer C., Fox-Kemper B., Kay J. E., Kinnison D., Kushner P. J., Larson V. E., Long M. C., Mickelson  
481 S., Moore J. K., Nienhouse E., Polvani L., Rasch P. J., and W. G. Strand: The Community Earth System  
482 Model Version 2 (CESM2). *Journal of Advances in Modeling Earth Systems*, 12, e2019MS001916.  
483 [https://doi.org/ 10.1029/2019MS001916](https://doi.org/10.1029/2019MS001916), 2020.
- 484 Deser, C., Phillips, A., Bourdette, V., Bourdette V., and Teng H.: Uncertainty in climate change projections: the  
485 role of internal variability. *Clim Dyn* 38, 527–546 (2012), <https://doi.org/10.1007/s00382-010-0977-x>,  
486 2020.
- 487 Drijfhout, S., van Oldenborgh, G. J., and Cimadoribus, A.: Is a Decline of AMOC Causing the Warming Hole  
488 above the North Atlantic in Observed and Modeled Warming Patterns?, *Journal of Climate*, 25, 8373–8379,  
489 <https://doi.org/10.1175/JCLI-D-12-00490.1>, [http:// journals.ametsoc.org/doi/abs/10.1175/JCLI-D-12-00490.1](http://journals.ametsoc.org/doi/abs/10.1175/JCLI-D-12-00490.1), 2012.
- 491 DuVivier, A. K., Holland, M. M., Kay, J. E., Tilmes, S., Gettelman, A., and Bailey, D. A.: Arctic and Antarctic sea  
492 ice mean state in the Community Earth System Model Version 2 and the influence of atmospheric  
493 chemistry. *Journal of Geophysical Research: Oceans*, 125, e2019JC015934. [https://doi.org/](https://doi.org/10.1029/2019JC015934)  
494 [10.1029/2019JC015934](https://doi.org/10.1029/2019JC015934), 2020.
- 495 Eyring, V., Bony, S., Meehl, G. A., Senior, C. A., Stevens, B., Stouffer, R. J., and Taylor, K. E.: Overview of the  
496 Coupled Model Intercomparison Project Phase 6 (CMIP6) experimental design and organization, *Geosci.*  
497 *Model Dev.*, 9, 1937–1958, <https://doi.org/10.5194/gmd-9-1937-2016>, 2016.
- 498 Gettelman, A., Mills, M. J., Kinnison, D. E., Garcia, R. R., Smith, A. K., Marsh, D. R., Times, S., Vitt F., Bardeen  
499 C. G., McInerny J., Liu H.-L., Solomon S.C., Polvani L. M., Emmons L. K., Lamarque J.-F., Richter, J. H.,  
500 Glanville A. S., Bacmeister J. T., Philips A. S., Neale R. B., Simpson I. R., DuVivier A. K., Hodzic A.,  
501 and Randel W. J.: The whole atmosphere community climate model version 6 (WACCM6). *Journal of*  
502 *Geophysical Research: Atmospheres*, 124, 12,380–12,403. [https://doi.org/ 10.1029/2019JD030943](https://doi.org/10.1029/2019JD030943), 2019.
- 503 Gettelman, A., and Morrison, H.: Advanced two-moment bulk microphysics for global models. Part I: Off-line  
504 tests and comparison with other schemes. *Journal of Climate*, 28, 1268–1287, [https://doi.org/10.1175/JCLI-](https://doi.org/10.1175/JCLI-D-14-00102.1)  
505 [D-14-00102.1](https://doi.org/10.1175/JCLI-D-14-00102.1), 2015.
- 506 Golaz, J.-C., Larson, V. E., and Cotton, W. R.: A PDF-based model for boundary layer clouds. Part I: Method and  
507 model description. *Journal of the Atmospheric Sciences*, 59, 3540–3551, 2002.
- 508 Hausfather, Z. and G. P. Peters: Emissions - ‘business as usual’ story is misleading. *Nature* 577, 618-620 (2020),  
509 doi: <https://doi.org/10.1038/d41586-020-00177-3>, 2020.



- 510 Hunke, E. C., Hebert, D. A., and Lecomte, O.: Level-ice melt ponds in the Los Alamos sea ice model, CICE.  
511 Ocean Modelling, 71, 26–42, <https://doi.org/10.1016/j.ocemod.2012.11.008>, 2013.
- 512 Hunke, E. C., Lipscomb, W. H., Turner, A. K., Jeffery, N., and Elliott, S.: CICE: The Los Alamos Sea Ice Model.  
513 Documentation and Software User's Manual. Version 5.1. T-3 Fluid Dynamics Group, Los Alamos  
514 National Laboratory, Tech. Rep. LA-CC-06-012, 2015.
- 515 IPCC: Global Warming of 1.5°C. An IPCC Special Report on the impacts of global warming of 1.5°C above pre-  
516 industrial levels and related global greenhouse gas emission pathways, in the context of strengthening the  
517 global response to the threat of climate change, sustainable development, and efforts to eradicate poverty  
518 [Masson-Delmotte, V., P. Zhai, H.-O. Pörtner, D. Roberts, J. Skea, P.R. Shukla, A. Pirani, W. Moufouma-  
519 Okia, C. Péan, R. Pidcock, S. Connors, J.B.R. Matthews, Y. Chen, X. Zhou, M.I. Gomis, E. Lonnoy, T.  
520 Maycock, M. Tignor, and T. Waterfield (eds.)]. 2018.
- 521 IPCC: Climate Change 2021: The Physical Science Basis. Contribution of Working Group I to the Sixth  
522 Assessment Report of the Intergovernmental Panel on Climate Change [Masson-Delmotte, V., P. Zhai, A.  
523 Pirani, S. L. Connors, C. Péan, S. Berger, N. Caud, Y. Chen, L. Goldfarb, M. I. Gomis, M. Huang, K.  
524 Leitzell, E. Lonnoy, J. B. R. Matthews, T. K. Maycock, T. Waterfield, O. Yelekçi, R. Yu and B. Zhou  
525 (eds.)]. Cambridge University Press. 2021.
- 526 Kay, J. E., Deser, C., Phillips, A., Mai, A., Hannay, C., Strand, G., Arblaster, J. M., Bates, S. C., Danabasoglu, G.,  
527 Edwards, J., Holland, M., Kushner, P., Lamarque, J.-F., Lawrence, D., Lindsay, K., Middleton, A., Munoz,  
528 E., Neale, R., Oleson, K., Polvani, L., and Vertenstein, M.: The Community Earth System Model (CESM)  
529 Large Ensemble Project: A Community Resource for Studying Climate Change in the Presence of Internal  
530 Climate Variability, *Bulletin of the American Meteorological Society*, 96(8), 1333-1349, 2015.
- 531 Keil, P., Mauritsen, T., Jungclaus, J. Hedemann C., Olonscheck D., and Ghosh R.: Multiple drivers of the North  
532 Atlantic warming hole. *Nat. Clim. Chang.* 10, 667–671, <https://doi.org/10.1038/s41558-020-0819-8>, 2020.
- 533 Kravitz, B., Caldeira K., Boucher O., Robock A., Rasch P. J., Alterskjær K., Karam D. B., Cole J. N. S., Curry C. L.  
534 , Haywood J. M., Irvine P. J., Ji D., Jones A., Kristjánsson J. E., Lunt D. J., Moore J. C., Niemeier U.,  
535 Schmidt H., Schulz M., Singh B., Tilmes S., Watanabe S., Yang S., and Yoon J.-H.: Climate model response  
536 from the Geoengineering Model Intercomparison Project (GeoMIP), *J. Geophys. Res. Atmos.*, 118, 8320–  
537 8332, doi:10.1002/jgrd.50646, 2013.
- 538 Kravitz, B., MacMartin, D. G., Vioni, D., Boucher, O., Cole, J. N. S., Haywood, J., Jones, A., Lurton, T., Nabat,  
539 P., Niemeier, U., Robock, A., Seferian, R., and Tilmes, S.: Comparing different generations of idealized  
540 solar geoengineering simulations in the Geoengineering Model Intercomparison Project (GeoMIP),  
541 *Atmospheric Chemistry and Physics*, 21, 4231-4247, <https://doi.org/10.5194/acp-21-4231-2021>, 2021.



- 542 Kravitz, B., MacMartin, D. G., Mills, M. J., Richter, J. H., Tilmes, S., Lamarque, J.-F., J. J. Tribbia, and Vitt, F.:  
543 First simulations of designing stratospheric sulfate aerosol geoengineering to meet multiple simultaneous  
544 climate objectives. *Journal of Geophysical Research: Atmospheres*, 122, 12,616–12,634,  
545 <https://doi.org/10.1002/2017JD026874>, 2017.
- 546 Larson, V. E., CLUBB-SILHS: A parameterization of subgrid variability in the atmosphere. arXiv:1711.03675v2  
547 [physics.ao-ph], 2017.
- 548 Lawrence, D. M., Fisher, R. A., Koven, C. D., Oleson, K. W., Swenson, S. C., Bonan, G., Collier N., Ghimire B.,  
549 van Kampenhout L., Kennedy D., Kluzek E., Lawrence P. J., Li F., Li H., Lombardozzi D., Riley W. J.,  
550 Sacks W. J., Shi M., Vertenstein M., Wieder W. R., Xu C., Ali A. A., Badger A. M., Bisht G., van den  
551 Broeke M., Brunke M. A., Burns S. P., Buzan J., Clark M., Craig A., Dahlin K., Drewniak B., Fisher J. B.,  
552 Flanner M., Fox A. M., Gentine P., Hoffman F., Keppel-Aleks G., Knox R., Kumar S., Lenaerts J., Leung  
553 L. R., Lipscomb W. H., Lu Y., Pandey A., Pelletier J. D., Perket J., Randerson J. T., Ricciuto D. M.,  
554 Sanderson B. M., Slater A., Subin Z. M., Tang J., Thomas R. Q., Val Martin M., and Zeng Z: The  
555 Community Land Model Version 5: Description of new features, benchmarking, and impact of forcing  
556 uncertainty. *Journal of Advances in Modeling Earth Systems*, 11, 4245–4287.  
557 <https://doi.org/10.1029/2018MS001583>, 2019.
- 558 Lee, W. , D. MacMartin, D. Visioni, and Kravitz B.: Expanding the design space of stratospheric aerosol  
559 geoengineering to include precipitation-based objectives and explore trade-offs. *Earth Syst. Dynam.*,11,  
560 1051-1072, <https://doi.org/10.5194/esd-11-1051-2020>, 2022.
- 561 Levis, S., Badger, A., Drewniak, B., Nevison, C., and Ren, X. L.: CLMcrop yields and water requirements:  
562 Avoided impacts by choosing RCP 4.5 over 8.5. *Climatic Change*, 146, 501–515,  
563 <https://doi.org/10.1007/s10584-016-1654-9>, 2018.
- 564 Li, H. Y., Wigmosta, M. S., Wu, H., Huang, M. Y., Ke, Y. H., Coleman, A. M., & Leung, L. R.: A physically  
565 based runoff routing model for land surface and Earth system models. *Journal of Hydrometeorology*, 14,  
566 808–828, <https://doi.org/10.1175/Jhm-D-12-015.1>, 2013.
- 567 Li, F., Levis, S., and Ward, D. S.: Quantifying the role of fire in the Earth system—Part 1: Improved global fire  
568 modeling in the Community Earth System Model (CESM1). *Biogeosciences*, 10, 2293–2314.  
569 <https://doi.org/10.5194/bg-10-2293-2013>, 2013.
- 570 Li, F., and Lawrence, D. M.: Role of fire in the global land water budget during the twentieth century due to  
571 changing ecosystems. *Journal of Climate*, 30, 1893–1908. <https://doi.org/10.1175/JCLI-D-16-0460.1>, 2017.



- 572 Liu, X., Ma, P. L., Wang, H., Tilmes, S., Singh, B., Easter, R. C., et al.: Description and evaluation of a new four-  
573 mode version of the Modal Aerosol Module (MAM4) within Version 5.3 of the Community Atmosphere  
574 Model. *Geoscientific Model Development*, 9, 505–522. <https://doi.org/10.5194/gmd-9-505-2016>, 2016.
- 575 MacMartin, D. G., Kravitz, B., Keith, D. W., and Jarvis, A.: Dynamics of the coupled human-climate system  
576 resulting from closed-loop control of solar geoengineering. *Climate Dynamics*, 43, 243–258. 2014.
- 577 MacMartin, D. G., Wang, W., Kravitz, B., Tilmes, S., Richter, J. H., and Mills, M. J.: Timescale for detecting  
578 the climate response to stratospheric aerosol geoengineering. *Journal of Geophysical Research:*  
579 *Atmospheres*, 124, 1233–1247. <https://doi.org/10.1029/2018JD028906>, 2019.
- 580 Maher, N., Milinski, S., and Ludwig, R.: Large ensemble climate model simulations: introduction, overview, and  
581 future prospects for utilising multiple types of large ensemble, *Earth Syst. Dynam.*, 12, 401–418,  
582 <https://doi.org/10.5194/esd-12-401-2021>, 2021.
- 583 Meehl, G. A., Arblaster, J. M., Bates, S., Richter, J. H., Tebaldi, C., Gettelman, A., et al.: Characteristics of future  
584 warmer base states in CESM2. *Earth and Space Science*, 7, e2020EA001296. [https://doi.](https://doi.org/10.1029/2020EA001296)  
585 [org/10.1029/2020EA001296](https://doi.org/10.1029/2020EA001296), 2020.
- 586 Mills, M. J., Richter, J. H., Tilmes, S., Kravitz, B., MacMartin, D. G., Glanville, A. A., Tribbia J. T., Lamarque  
587 J-F., Vitt F., Schmidt A., Gettelman A., Hannay C., Bacmeister J. T., and Kinnison, D. E.: Radiative and  
588 chemical response to interactive stratospheric sulfate aerosols in fully coupled CESM1(WACCM). *Journal*  
589 *of Geophysical Research: Atmospheres*, 122, 13,061–13,078, <https://doi.org/10.1002/2017JD027006>,  
590 2017.
- 591 Moore, J. K., Doney, S. C., Kleypas, J. A., Glover, D. M., and Fung, I. Y.: An intermediate complexity marine  
592 ecosystem model for the global domain. *Deep Sea Research*, 49, 403–462. [https://doi.org/10.1016/S0967-](https://doi.org/10.1016/S0967-0645(01)00108-4)  
593 [0645\(01\)00108-4](https://doi.org/10.1016/S0967-0645(01)00108-4), 2002.
- 594 Moore, J. K., Doney, S. C., and Lindsay, K.: Upper ocean ecosystem dynamics and iron cycling in a global three-  
595 dimensional model. *Global Biogeochemical Cycles*, 18, GB4028. <https://doi.org/10.1029/2004GB002220>,  
596 2004.
- 597 Moore, J. K., Lindsay, K., Doney, S. C., Long, M. C., & Misumi, K. Marine Ecosystem Dynamics and  
598 Biogeochemical Cycling in the Community Earth System Model [CESM1(BGC)]: Comparison of the  
599 1990s with the 2090s under the RCP4.5 and RCP8.5 scenarios. *Journal of Climate*, 26, 9291–9312.  
600 <https://doi.org/10.1175/JCLI-D-12-00566.1>, 2013.



- 601 National Academies of Sciences, Engineering, and Medicine. Reflecting Sunlight: Recommendations for Solar  
602 Geoengineering Research and Research Governance. Washington, DC: The National Academies Press.  
603 <https://doi.org/10.17226/25762>, 2021.
- 604 O'Neill, B. C., Tebaldi, C., Van Vuuren, D. P., Eyring, V., Friedlingstein, P., Hurtt, G., Knutti R., Kriegler E.,  
605 Lamarque J-F., Lowe J., Meehl G. A., Moss R., Riahi K., and Sanderson B. M.: The Scenario Model  
606 Intercomparison Project (ScenarioMIP) for CMIP6. Geoscientific Model Development, 9(9), 3461–3482,  
607 <https://doi.org/10.5194/gmd-9-3461-2016>, 2016.
- 608 Brian C. O'Neill, Elmar Kriegler, Kristie L. Ebi, Eric Kemp-Benedict, Keywan Riahi, Dale S. Rothman, Bas J. van  
609 Ruijven, Detlef P. van Vuuren, Joern Birkmann, Kasper Kok, Marc Levy, William Solecki: The roads  
610 ahead: Narratives for shared socioeconomic pathways describing world futures in the 21st century, Global  
611 Environmental Change, 42, 169-180, <https://doi.org/10.1016/j.gloenvcha.2015.01.004>, 2017.
- 612 Oleson, K. W., and Feddema, J. : Parameterization and surface data improvements and new capabilities for the  
613 Community Land Model Urban (CLMU). Journal of Advances in Modeling Earth Systems., 12,  
614 <https://doi.org/10.1029/2018MS001586>, 2019.
- 615 Pitari, G., Aquila V., Kravitz B., Robock A., Watanabe S., Cionni I., De Luca N., Di Geonva G., Mancini E., and  
616 Tilmes S.: Stratospheric ozone response to sulfate geoengineering: Results from the Geoengineering Model  
617 Intercomparison Project (GeoMIP). J. Geophys. Res. Atmos., 119, 2629–2653,  
618 <https://doi.org/10.1002/2013JD020566>, 2014.
- 619 Richter, J. H., Sassi, F., and Garcia, R. R.: Toward a Physically Based Gravity Wave Source Parameterization in a  
620 General Circulation Model. Journal of the Atmospheric Sciences, 67(1), 136–156,  
621 <https://doi.org/10.1175/2009JAS3112.1>, 2010.
- 622 Richter, J. H., Tilmes, S., Mills, M. J., Tribbia, J., Kravitz, B., MacMartin, D. G., Vitt, F., and Lamarque J-F.:  
623 Stratospheric dynamical response and ozone feedbacks in the presence of SO<sub>2</sub> injections. Journal of  
624 Geophysical Research: Atmospheres, 122, 12,557–12,573, <https://doi.org/10.1002/2017JD026912>, 2017.
- 625 Scinocca, J., and Mcfarlane N.: The parametrization of drag induced by stratified flow over anisotropic orography.  
626 Quarterly Journal of the Royal Meteorological Society, 126, 2353–2394,  
627 <https://doi.org/10.1256/smsqj.56801>, 2000.
- 628 Simpson, I. R., Tilmes, S., Richter, J. H., Kravitz, B., MacMartin, D. G., Mills, M. J., Fasullo J. T., and  
629 Pendergrass A. G.: The regional hydroclimate response to stratospheric sulfate geoengineering and the role  
630 of stratospheric heating. Journal of Geophysical Research: Atmospheres, 124, 12587– 12616,  
631 <https://doi.org/10.1029/2019JD031093>, 2019.



- 632 Simpson, I. R., Bacmeister, J., Neale, R. B., Hannay, C., Gettelman, A., Garcia, R. R., Lauritzen P. H., March D.  
633 R., Mills M. J., Medeiros B., and Richter J. H.: An evaluation of the large-scale atmospheric circulation and  
634 its variability in CESM2 and other CMIP models. *Journal of Geophysical Research: Atmospheres*, 125,  
635 e2020JD032835, [https://doi.org/ 10.1029/2020JD032835](https://doi.org/10.1029/2020JD032835), 2020.
- 636 Smith, R., Jones P., Briegleb B., Bryan F., Danabasoglu G., Dennis J., Dukowicz J., Eden C., Fox-Kemper B., Gent  
637 P., Hecht M., Jayne S., Jochum M., Large W., Lindsay K., Maltrud M., Norton N., Peacock S., Vertenstein  
638 M., Year S.: The Parallel Ocean Program (POP) reference manual, Ocean component of the Community  
639 Climate System Model (CCSM), LANL Technical Report, LAUR-10-01853, 141 pp., 2010.
- 640 Tebaldi, C., Debeire, K., Eyring, V., Fischer, E., Fyfe, J., Friedlingstein, P., Knutti, R., Lowe, J., O'Neill, B.,  
641 Sanderson, B., van Vuuren, D., Riahi, K., Meinshausen, M., Nicholls, Z., Tokarska, K. B., Hurtt, G.,  
642 Kriegler, E., Lamarque, J.-F., Meehl, G., Moss, R., Bauer, S. E., Boucher, O., Brovkin, V., Byun, Y.-H.,  
643 Dix, M., Gualdi, S., Guo, H., John, J. G., Kharin, S., Kim, Y., Koshiro, T., Ma, L., Olivie, D., Panickal, S.,  
644 Qiao, F., Rong, X., Rosenbloom, N., Schupfner, M., Séférian, R., Sellar, A., Semmler, T., Shi, X., Song, Z.,  
645 Steger, C., Stouffer, R., Swart, N., Tachiiri, K., Tang, Q., Tatebe, H., Voldoire, A., Volodin, E., Wyser, K.,  
646 Xin, X., Yang, S., Yu, Y., and Ziehn, T.: Climate model projections from the Scenario Model  
647 Intercomparison Project (ScenarioMIP) of CMIP6, *Earth Syst. Dynam.*, 12, 253–293,  
648 <https://doi.org/10.5194/esd-12-253-2021>, 2021.
- 649 Tilmes, S., Richter, J. H., Kravitz, B., MacMartin, D. G., Mills, M. J., Simpson, I. R., Glanville, A. S., Fasullo, J.  
650 T., Phillips, A. S., Lamarque, J., Tribbia, J., Edwards, J., Mickelson, S., and Ghosh, S.: CESM1(WACCM)  
651 Stratospheric Aerosol Geoengineering Large Ensemble Project, *Bulletin of the American Meteorological*  
652 *Society*, **99**(11), 2361–2371, 2018.
- 653 Tilmes, S., Mills, M. J., Niemeier, U., Schmidt, H., Robock, A., Kravitz, B., Lamarque, J.-F., Pitari, G., and  
654 English, J. M.: A new Geoengineering Model Intercomparison Project (GeoMIP) experiment designed for  
655 climate and chemistry models, *Geosci. Model Dev.*, 8, 43–49, <https://doi.org/10.5194/gmd-8-43-2015>,  
656 2015.
- 657 Tilmes S., Richter J. H., Mills M. J., Kravitz B., MacMartin D. G., Vitt F., Tribbia J. T., Lamarque J.-F.: Sensitivity  
658 of aerosol distribution and climate response to stratospheric SO<sub>2</sub> injection locations, *Journal of Geophysical*  
659 *Research: Atmospheres*, 122, 12,591– 12,615. <https://doi.org/10.1002/2017JD026888>, 2017.
- 660 Tolman, H. L.: User manual and system documentation of WAVEWATCH III TM version 3.14. Technical note,  
661 MMAB Contribution, 276, p.220., 2009.
- 662 Tye, M. R., Dagon, K., Molina, M. J., Richter, J. H., Visioni, D., Kravitz, B., Tebaldi, C., and Tilmes, S.: Indices of  
663 Extremes: Geographic patterns of change in extremes and associated vegetation impacts under climate intervention,  
664 *EGUsphere* [preprint], <https://doi.org/10.5194/egusphere-2022-1>, 2022



- 665 Visioni, D., MacMartin, D. G., and Kravitz B.: Is Turning Down the Sun a Good Proxy for Stratospheric Sulfate  
666 Geoengineering?, *Journal of Geophysical Research: Atmospheres*, 126, e2020JD033952, 2021a.
- 667 Visioni, D., MacMartin, D. G., Kravitz, B., Boucher, O., Jones, A., Lurton, T., Martine, M., Mills, M. J., Nabat, P.,  
668 Niemeier, U., Séférian, R., and Tilmes, S.: Identifying the sources of uncertainty in climate model  
669 simulations of solar radiation modification with the G6sulfur and G6solar Geoengineering Model  
670 Intercomparison Project (GeoMIP) simulations, *Atmos. Chem. Phys.*, 21, 10039–10063,  
671 <https://doi.org/10.5194/acp-21-10039-2021>, 2021b.
- 672 Zhang, G. J., and McFarlane, N. A.: Sensitivity of climate simulations to the parameterization of cumulus  
673 convection in the Canadian Climate Center general circulation model. *Atmosphere-Ocean*, 33, 407–446,  
674 1995.
- 675